Soft Matter

ARTICLE

On skin microrelief and the emergence of expression micro-wrinkles

Received 00th January 20xx,
Accepted 00th January 20xx

DOI: 10.1039/x0xx00000x

www.rsc.org/softmatter

G. Limbert*[a,b] and E. Kuhl[c]

Over the course of a life time, as a result of adaptive mechanobiological processes (e.g. ageing), or the action of external physical factors such as mechanical loading, the human skin is subjected to, and hosts complex biophysical processes. These phenomena typically operate through a complex interplay, that, ultimately, is responsible for the evolutive geometrical characteristics of the skin surface. Wrinkles are a manifestation of these effects. Although numerous theoretical models of wrinkles arising in multi-layered structures have been proposed, they typically apply to idealised geometries. In the case of skin, which can be viewed as a geometrically complex multi-layer assembly, it is pertinent to question whether the natural skin microrelief could play a significant role in conditioning the characteristics of compression-induced micro-wrinkles by acting as an array of geometrical imperfections. Here, we explore this question through the development of an anatomically-based finite strain parametric finite element model of the skin, represented as a *stratum corneum* layer on top of a thicker and softer substrate. Our study suggests that skin microrelief could be the dominant factor conditioning micro-wrinkle characteristics for moderate elastic modulus ratios between the two layers. Beyond stiffness ratios of 100, other factors tend to overwrite the effects of skin microrelief. Such stiffness ratio fluctuations can be induced by changes in relative humidity or particular skin conditions and can therefore have important implications for skin tribology.

1 Introduction

In popular culture, skin wrinkles, particularly on the face, are the hallmark of ageing. They have been the subject of a large number of studies in the dermatological, surgical and cosmetic communities because of their societal importance in relation to health, age and beauty[1] but also, in the case of expression wrinkles (i.e. those mechanically-activated by facial muscle contraction), because of their role in conveying particular emotions and providing conscious and subconscious cues to support verbal language. This aspect is particularly crucial for modern computer graphics techniques used in the digital animation industry because of the public appetite for an ever growing level of physical realism for the simulated facial behaviour of animated characters[2-5]. Besides these important facets of human life, unveiling the underlying mechanical principles that condition the morphologies and patterns of wrinkles are essential in evaluating, and ultimately, predicting, how an ageing or aged skin interacts with its environment. This also holds the promise to provide insights into the physiology and biophysics of skin in health, disease, ageing and trauma[6].

Many products that interact with, support or protect human skin can actually cause discomfort to the user and even irritation or damage to the skin through excessive and/or ill-distributed load transmission. Friction is central[7-9] to these problems. Skin friction is typically decomposed into an adhesive and deformation-induced component[10-13]. Any alteration of the skin surface (e.g. wrinkles), particularly at the microscopic scale, is likely to modulate these effects[6, 8, 14]. Moreover, because ageing wrinkles are generally correlated with change in the physical, material and structural properties of the subjacent microstructural skin layers[15, 16], the tribological response of the skin is highly dependent upon wrinkle characteristics, and therefore age. For example, the mechanics of a razor sliding over the facial skin of a teenager and that of an elderly man with deeper micro-wrinkles and stiffer skin tend to have very different characteristics, particularly if lubrication and skin hydration[17] are introduced through the use of a shave preparation. The global and continuous rise of the aged population means that accounting for this type of biomechanical factors in the development of new products will become essential in the near future. Moreover, the growing market of stretchable and wearable epidermal electronics[18] put wrinkles in the spotlight as these systems which do not only interact with the skin and its topography, are also often multi-layer systems themselves which are prone to wrinkling behaviour[19].

From the view point of biomechanics, the skin is generally considered as a multi-layer assembly made up of three main structures: the epidermis, dermis and hypodermis[6, 20, 21].

[a] *National Centre for Advanced Tribology at Southampton | Bioengineering Research Group, Faculty of Engineering and the Environment, University of Southampton, University Road, Southampton, SO17 1BJ, UK. Email: g.limbert@soton.ac.uk.*
[b] *Biomechanics and Mechanobiology Laboratory, Division of Biomedical Engineering, Department of Human Biology, Faculty of Health Sciences, University of Cape Town, Observatory 7935, South Africa.*
[c] *Department of Mechanical Engineering | Department of Bioengineering | Department of Cardiothoracic Surgery, Stanford University, Stanford CA 94305, USA. Email: ekuhl@stanford.edu.*

In order to develop a mechanistic understanding of skin wrinkles it is therefore natural to treat it as a tri- or bi-layer structure[22] and rely on appropriate mathematical theories and computational approaches to surface instability phenomena. However, despite the large body of work on surface instabilities conducted in the last fifteen years[19, 22-30], the majority of mathematical models are often restricted to idealised conditions (e.g. perfectly flat rectilinear structures, i.e. plates). Although these models have offered tremendous physical insight into various types of surface instabilities pertaining to engineered and biological systems, including wrinkling[22, 24, 31], folding[32], creasing[29] and cusping[33], their applicability beyond their intrinsic domain of validity might be called into question. For example, Cao and Hutchinson[29] highlighted the strong imperfection-sensitivity of wrinkles in bi-layer structures featuring a thin film laying on top of an infinite half-space substrate. It is therefore relevant to consider whether the natural geometrically complex microstructure of the human skin could lead to compression-induced wrinkles that would deviate from the theoretical solutions obtained for equivalent idealised multi-layer structures. Of particular significance is the three-dimensional skin surface topography, also known as *microrelief*[1] that will be described in more details below. It is part of the outermost layer of skin, the *stratum corneum*, a 10 to 30 µm-thick layer of dead keratinocytes bonded by desmosomes, the viable epidermis which contains living cells, and to a certain extent, the papillary and reticular dermis (**Figure 1**)[20].

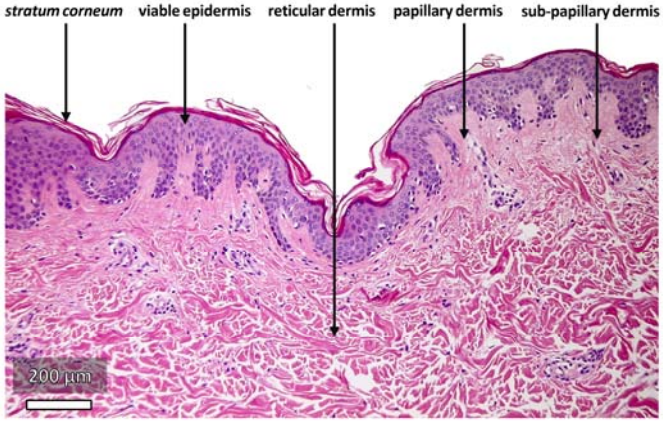

Figure 1. Histological section of haematoxylin and eosin stained back human skin sample highlighting its different structural layers. Adapted from Limbert[6]. Courtesy of Dr. Maria Fabiola Leyva-Mendivil, University of Southampton.

Moreover, the interplay between the structural characteristics and material properties of the skin layers and its role on wrinkle formation have not been explored other than for highly idealised conditions[34] and/or situations considering wrinkles at a macroscopic length scale[35, 36]. *Skin wrinkles* (or *skin folds*, in the *clinical* sense)[1] are generally associated with ageing and manifest themselves as amplification of the natural skin microrelief. There is evidence that ageing wrinkles do not arise from the emergence of new skin structures but are merely a manifestation of alterations in the material and structural properties of the skin caused by intrinsic and extrinsic ageing[37, 38].

In addition to these effects, there is also adaptation (i.e. growth/resorption) of the underlying anatomical structures including adipose tissues, muscles and bones whilst the mechanical environment of the dermal tissue is also evolving (e.g. relaxation of tension along Langer lines). *Expression (or temporary) wrinkles* (also called *expression lines*) are typically associated with facial skin movement and are rather macroscopic in nature. They can originate from facial muscular activation (i.e. smiling) or by mechanical actions on the skin surface such as twisting, shear or compression. In this study, we will consider dynamic wrinkles at a smaller scale, that of skin microrelief, which are also induced by in-plane compression of the skin. Henceforth, they will be referred as *micro-wrinkles* (MW). The focus is on this type of wrinkles because they play a key role in modulating the frictional response of the skin[10, 13]

Skin microrelief (**Figure 2**) is made of a network of furrows and ridges—also called *sulcus cutis* or glyphic patterns—criss-crossing each other and thus delimiting polygonal plateaux with rectangular, square, trapezoidal and triangular shapes. These polygonal patterns—present at birth—lose their isotropic distribution with age and become more anisotropic by forming preferred structural orientations [39-41]. The characteristics of skin microrelief can be classified according to the orientation and depth of featured lines into primary, secondary, tertiary and quaternary lines [39, 40, 42-45] (**Figure 2**). The primary lines are wide and deep (30 to 100 µm relative to the skin surface) while the secondary lines are narrower and shallower than the former (5 to 40 µm)[44]. The thin micro-topography that delineates the edges of corneocytes on the skin surface give rise to the tertiary lines while the quaternary lines are constituted by the thinner irregular bulges (blebs) and trabecular networks on the corneocyte membrane itself[45]. As part of the ageing process, the depth of primary lines can deepen to several hundreds of micrometers to form wrinkles. In young skin, the grooves formed by the skin glyphic patterns are shallow and closely spaced while this trend is reversed in aged skin[46].

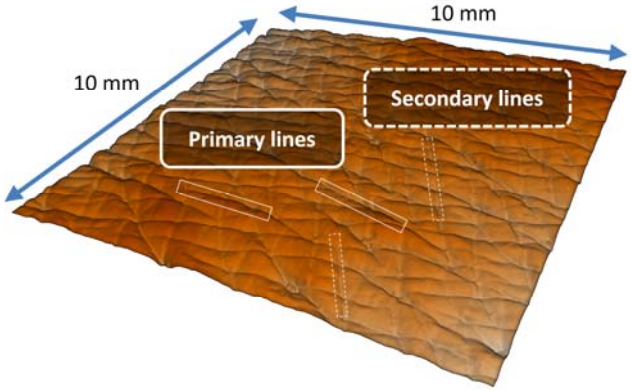

Figure 2 Synthetic image representing the typical microrelief of the skin surface (ridges and furrows), reconstructed from laser scanning profilometry of a silicone replica of a human volar forearm skin patch. Some of the primary and secondary lines are delineated and overlaid over the skin surface. The acquisition features a 400 x 400 grid of points that was fitted to a NURBS surface.

As alluded above, the link between skin microrelief and the geometrical and mechanical characteristics of compression-induced MW remains elusive. Can human skin be considered as a multi-layer plate structure when studying its wrinkling behaviour? In which conditions does this assumption break down? Are the structural features of skin microrelief key imperfections that favour particular instability modes? How does the stiffness of *stratum corneum* affect this type of non-linear phenomena? Unravelling the link between the characteristics of skin microrelief and its evolution during the formation of MW is key in gaining a fundamental mechanistic insight into how humans mechanically interact with their natural and engineered environments.

Addressing aspects of these fundamental questions constituted the prime motivation of the present study. Some of these ideas were explored through the development and exploitation of an anatomically-based parametric finite element multi-layer skin model. The skin was modelled as a two-layer neo-Hookean composite structure. This two-layer approach was selected for two reasons. First, although very thin (10 to 30 μm), the *stratum corneum* can be a major contributor to the mechanics of the epidermis[10, 11, 35, 47] because of its ability to stiffen by up to three orders of magnitude, in a matter of hours, when relative humidity levels drop from 100 to 0%[17, 48, 49]. For in-plane compression, the collagen fibre-rich dermis, which is the main load-bearing structural component of the skin in tension, is unlikely to resist much compressive loads. It is therefore reasonable to assume that, in these conditions, the *stratum corneum* would be the main resisting structural element whilst the underlying layers (i.e. viable epidermis and dermis) would behave as highly compliant layers featuring similar isotropic mechanical properties. These layers could therefore be assumed to form a homogeneous thick substrate. The second reason for considering a two-layer structure is to focus on the effects of skin microrelief geometry on wrinkle formation and characteristics, without introducing unnecessary complexity that would make interpretation of results less direct.

The central hypothesis underpinning the study presented here is that the characteristics of compression-induced wrinkles are primarily determined by the natural skin microrelief rather than the ratio of stiffness if one considers skin as a *stratum corneum*-soft substrate structure. A slightly more refined hypothesis is that this might only be true below a critical level of stiffness ratio.

In **section 2,** the general modelling methodology to build an anatomically-based skin model to simulate compression-induced wrinkling is presented while results of the parametric finite element analyses are analysed and discussed in **section 3**. Finally, conclusions to the study are drawn in **section 4**.

2 Modelling

In this section, we introduce the methodology used to create an anatomically-based finite element multi-layer skin model and the associated parametric finite element analyses designed to study the material and structural role of skin microrelief on the characteristics of compression-induced MW.

Experimentally-based finite element model generation

Critical to our study, in order to incorporate a realistic skin surface topography geometry, a quick-setting silicone (DAV0633 Silflo®, JS Davis, Stevenage, UK) replica of a patch of volar forearm skin of a 40 years-old male subject volunteer with no skin condition (including dryness) was casted. This followed standard skin profilometric characterisation using non-contact optical techniques [50, 51]. A representative 10 mm x 10 mm region of interest was identified on the skin replica and scanned using a triangulation laser profilometer Xyris 2000 TL (Taicaan Technologies, Southampton, UK).

From the profilometric acquisition, an ASCII file containing a regular grid of 400 x 400 points and their respective spatial coordinates was generated, providing an XY spatial resolution of 25 μm (**Figure 2**). The file was imported into Mathematica® 10.0 (Wolfram Research, Inc., Champaign, IL, USA.) where a three-dimensional structured eight-noded hexahedron-based multi-layer finite element mesh was generated. To minimise the effect of surface curvature, a 5 mm x 5 mm subset region was selected. The *stratum corneum* layer was assumed to be a 20 μm uniformly-thick structure[52] while the underlying layers (viable epidermis, papillary and reticular dermis) were represented by a 2.6 mm thick single layer (**Figure 3**). Nodes at the interface between the *stratum corneum* and underlying substrate were congruent to enforce perfect bonding.

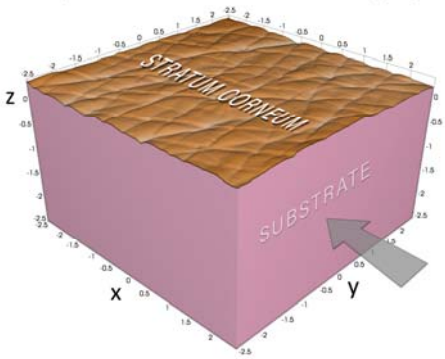

Figure 3 Solid rendering of the anatomically-based finite element bi-layer model of the skin featuring a 20 μm uniformly-thick *stratum corneum* laying on a 2.6 mm thick substrate. The displacement boundary condition is indicated by a grey arrow.

Constitutive modelling

Each of the two layers was assigned its own mechanical properties obeying a constitutive law based on a neo-Hookean elastic potential ψ [53]:

$$\psi = \frac{E}{4(1+\nu)}\left(\mathbf{b}:\mathbf{I}-3-2\ln J\right)+\frac{E\nu}{2(1+\nu)(1-2\nu)}\ln^2(J) \quad (1)$$

where $\mathbf{b}$ and $\mathbf{I}$ are respectively the left Cauchy-Green deformation and identity tensors, E and ν, ground state Young's modulus and Poisson's ratio and $J=\det(\mathbf{b})^{1/2}$. The Kirchhoff stress tensor $\boldsymbol{\tau}$ is obtained by differentiation of the free energy ψ and push-forward operation[54]:

$$\boldsymbol{\tau} = 2\frac{\partial\psi}{\partial\mathbf{b}}\mathbf{b} = \frac{E}{2(1+\nu)}(\mathbf{b}-\mathbf{I})+\frac{E\nu}{(1+\nu)(1-2\nu)}\ln(J)\mathbf{I} \quad (2)$$

The equilibrium equation reads as:

$$\nabla.(J\boldsymbol{\tau})+\boldsymbol{f}_B = \rho\,\mathbf{a} \quad (3)$$

where f_B, ρ and $\mathbf{a}$ are respectively body forces, density and acceleration. A trilinear interpolation 8-noded hexahedral finite element featuring a "B-bar formulation"[55] to prevent volumetric locking was implemented within the AceFEM framework[56, 57] in Mathematica® (Wolfram Research, Inc., Champaign, IL, USA).

The mechanical properties of the substrate were maintained constant throughout the parametric study (Young's modulus: 0.6 MPa; Poisson's ratio: 0.45).

Young's modulus of the *stratum corneum* was varied from 0.6 to 360 MPa[47] (with a fixed Poisson's ratio of 0.45). The ratio of *stratum corneum* Young's modulus over that of the substrate is denoted $\alpha = E_{SC} / E_{substrate}$ (**Table 1**).

Table 1. Young's modulus ratios considered in the parametric finite element analysis and corresponding values of *stratum corneum* Young's modulus.

α	1	20	100	200	400	600
E_{SC} [MPa]	0.6	12	60	120	240	360

Computational procedure

To trigger wrinkle formation, a uniform uniaxial compressive displacement along the X-direction was applied to one vertical boundary face of the whole bi-layer domain (x = 2.5 mm). This 2.5 mm displacement corresponds to a 25% macroscopic strain (**Figure 3**). Symmetry conditions were enforced.

Wrinkling instabilities are highly non-linear phenomena and, as a result, very challenging to robustly model in a numerical context. Standard Newton-Raphson incremental solving procedures may fail[58], thus requiring better path-following procedures such as arc-length methods[59], asymptotic numerical techniques[60] and/or approaches based on dynamic regularisation. To continuously capture steep curvature gradients occurring in surface instabilities, isogeometric interpolation schemes appear to be superior to those based on Lagrange polynomials[61-63]. Identifying critical conditions that trigger surface instabilities is also a challenging endeavour and has therefore stimulated the development of new numerical analysis methods[64]. In this work, in order to stabilise an arc-length solution procedure, the standard Newmark[65] integration scheme was implemented. This approach effectively boils down to adding dynamic terms to the quasi-static formulation. The Newmark scheme parameters and velocities were adjusted such that the influence of the applied stabilisation on the solution was negligible.

3 Results and discussion

Results of the six finite element analyses, corresponding each to a particular value of Young's modulus for the *stratum corneum* (**Table 1**), were collected and analysed.

Figure 4 shows the deformed shape of the *stratum corneum* layer as a function of the stiffness ratio α. This factor has a significant influence on the wavelength and amplitude of wrinkles. Period-doubling phenomena[23, 66] occur from $\alpha = 100$ and evolve into more complex modes which suggest period-tripling.

When the *stratum corneum* and substrate layers have the same ground state elasticity moduli, the deformed skin profile is merely a magnification of natural skin microrelief: existing valleys get deeper and no new surface features are created although high curvature gradients are produced. Here, it should be emphasised that this observation is based on results that were obtained for a single microrelief sample. Different geometrical surface characteristics associated with different samples would likely lead to different structural deformations. However, the main point to consider is qualitative, namely the fact that surface imperfections trigger wrinkling modes that deviate for theoretical solutions obtained for idealised bi-layer structures. As α increases, its effect becomes dominant over that of the structural geometrical properties of the *stratum corneum* layer. To establish a direct link between microrelief characteristics and out-of-plane deformations (i.e. MW) a metric called *elevation ratio* is defined for every node of the external *stratum corneum* surface.

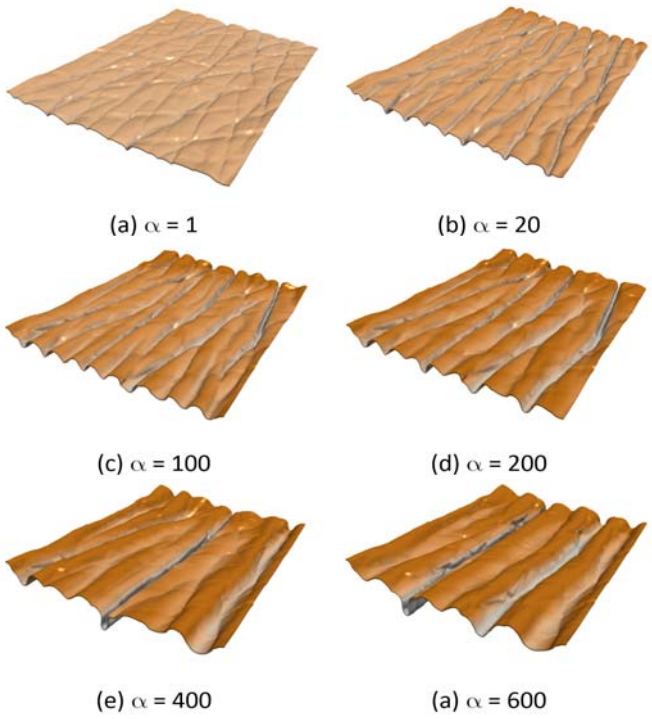

Figure 4 Deformed shape of the 20 µm uniformly-thick *stratum corneum* as a function of stiffness ratio α following a 25% macroscopic uniaxial compression.

It is the ratio of the position along the z-axis in the *deformed* configuration over that in the *undeformed* configuration. This could be viewed as an equivalent normal stretch along the z-axis. The elevation ratio is plotted for 3 separate vertical cross-sections corresponding to the middle and lateral portion of the multi-layer structure (**Figure 5**) and for four values of α only (1, 100, 400, 600) to maintain clarity of the graphic plots.

Besides the effect of α on out-of-plane deformations as highlighted in **Figure 4**, the direct correspondence between peaks and valleys of the undeformed external surface of the *stratum corneum* layer and the deformations of that surface is clearly visible, and also modulated by α. Upon application of compressive forces, peaks and valleys are magnified or switched into valleys and peaks.

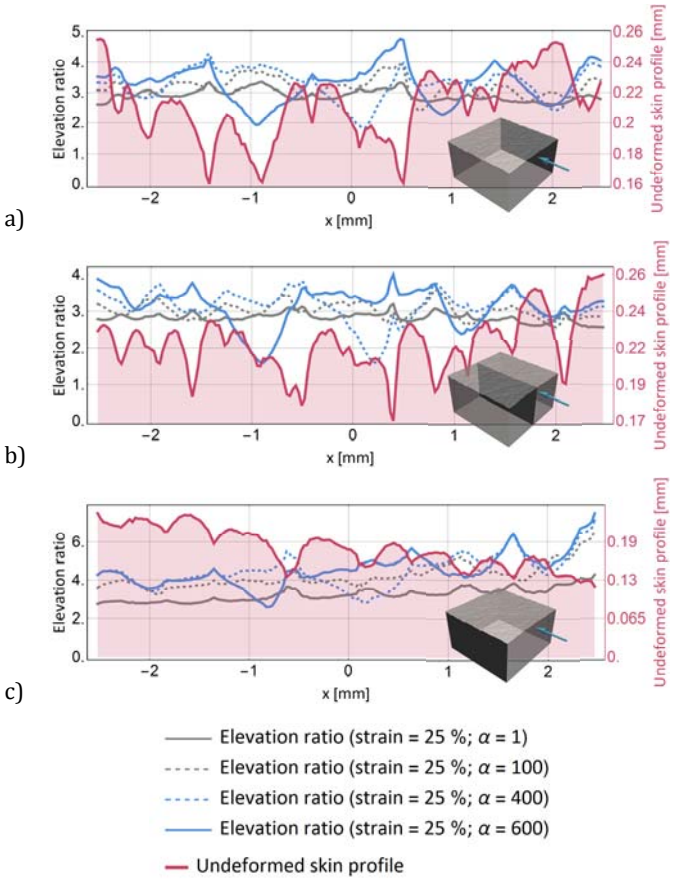

Figure 5. Distribution and magnitude of elevation ratio (out-of-plane stretch) of the skin outer surface (*stratum corneum*) for 25% compressive strain at three different locations along the y-axis (a) y = -2.5 mm; b) y = 0 mm; c) y = 2.5 mm).

The relative distribution of minimum principal strain magnitude at the surface of the skin with respect to the original topographical features (**Figure 6**) or in the full three-dimensional setting (**Figure 7**) as well as normal stress along the direction of compression (**Figure 8**) are useful measures to assess the role of microrelief on MW characteristics.

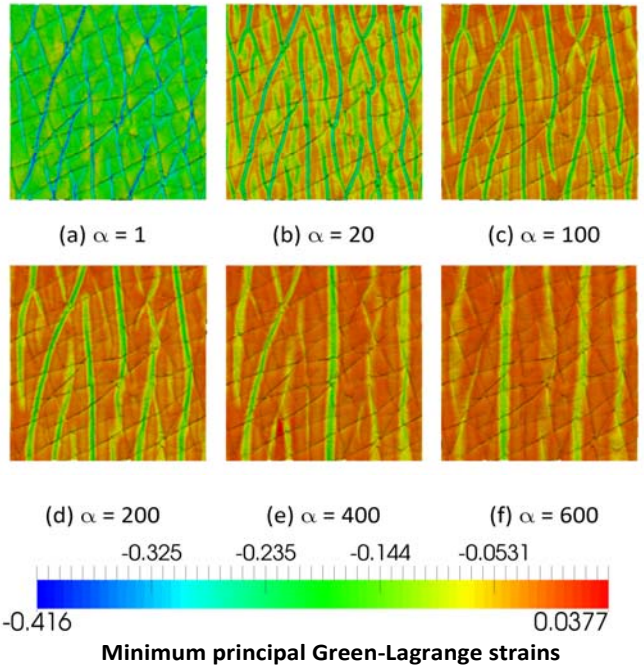

Figure 6 Colour plot of minimum principal Green-Lagrange strains at the surface of the *stratum corneum* after 25% compression as a function of α .

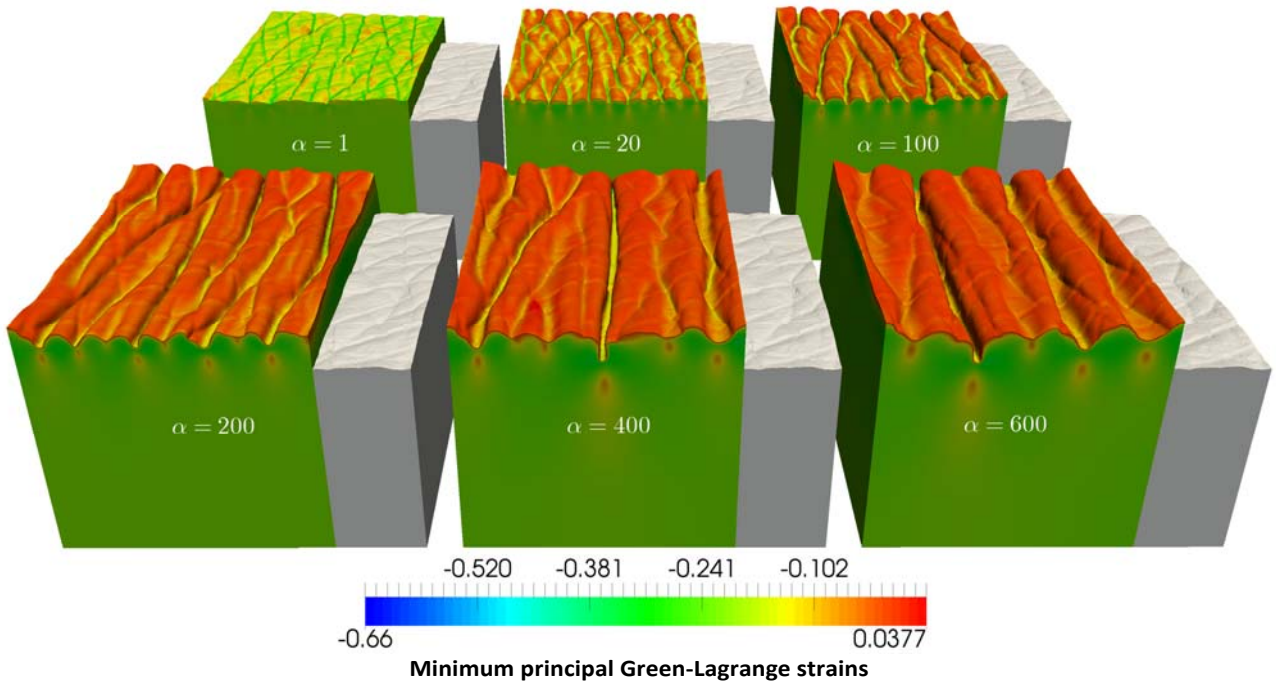

Figure 7 Colour plots of minimum principal Green-Lagrange strains after application of a 25% macroscopic uniform compressive strain for each value of the stiffness ratio α . The (white) undeformed skin geometry is overlaid over that of the deformed ones.

For moderate α values (≤100), secondary lines of skin microrelief can still act as imperfections triggering wrinkle formation. As α increases, these imperfections (including those represented by primary lines) become less dominant on wrinkle wavelength. Compressive and tensile principal strains also get progressively realigned along the direction normal to that of the applied compressive force. There is a clear correlation between the spatial frequency of wrinkles and α (**Figure 8**).

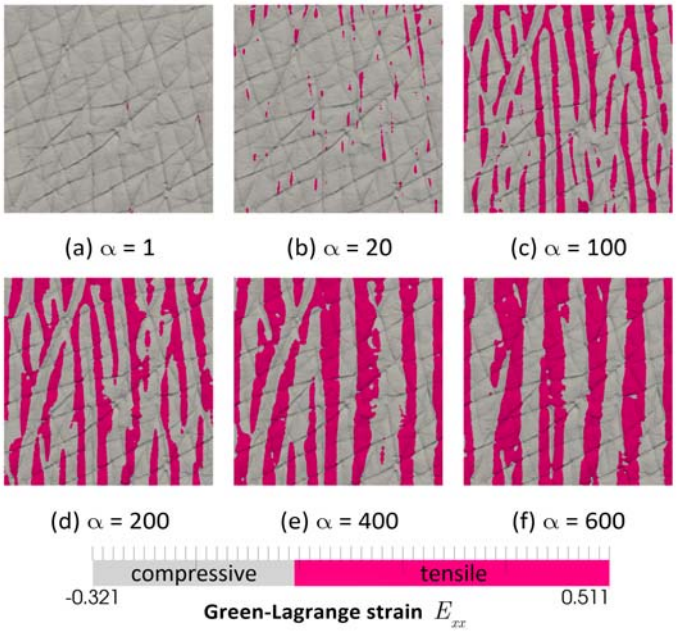

Figure 8 Distribution and magnitude of out-of-plane displacement of the skin outer surface (*stratum corneum*) projected on to the *undeformed* skin model.

In their experimentally-based computational model of compression-induced macroscopic skin wrinkles, Flynn and McCormack[35] provided a valuable insight into the influence of the number of skin layers and pre-stress on wrinkle formation. In both *in vitro* and *in silico* experiments, it was observed that the depth of wrinkles significantly increases under 20-30% strain. This model was subsequently used to simulate ageing effects on compressive wrinkle formation but did not take into account real skin microrelief[36]. Although our model is defined at a smaller length scale, significant deepening of wrinkles is also observed after application of a 25% macroscopic compressive strain, and this effect is magnified as α increases.

Three-dimensional characterisation of skin wrinkles

There exists a wide range of metrics to characterise the topography of a surface through sampling of its two-dimensional profiles[67]. Here, the focus is on determining the characteristic wavelengths of the compression-induced skin wrinkles and compare them to the theoretical solutions obtained for equivalent bilayer neo-Hookean structures. Using the same three vertical cutting planes co-linear with the uniaxial load direction as for Figure 4, the surface of the *stratum corneum* was sampled and the multiple wavelengths observed over each profile were determined by measuring the distance between peaks (**Figure 9**). The built-in Mathematica® function `FindPeaks`[68] was used to detect peaks. It is based on a Gaussian filter which identify peaks surviving a blurring up to a scale σ (here, chosen as σ = 25 μm).

As expected from physical intuition and theoretical models, **Figure 9** shows a clear increase of wrinkle wavelength with increasing stiffness ratio α.

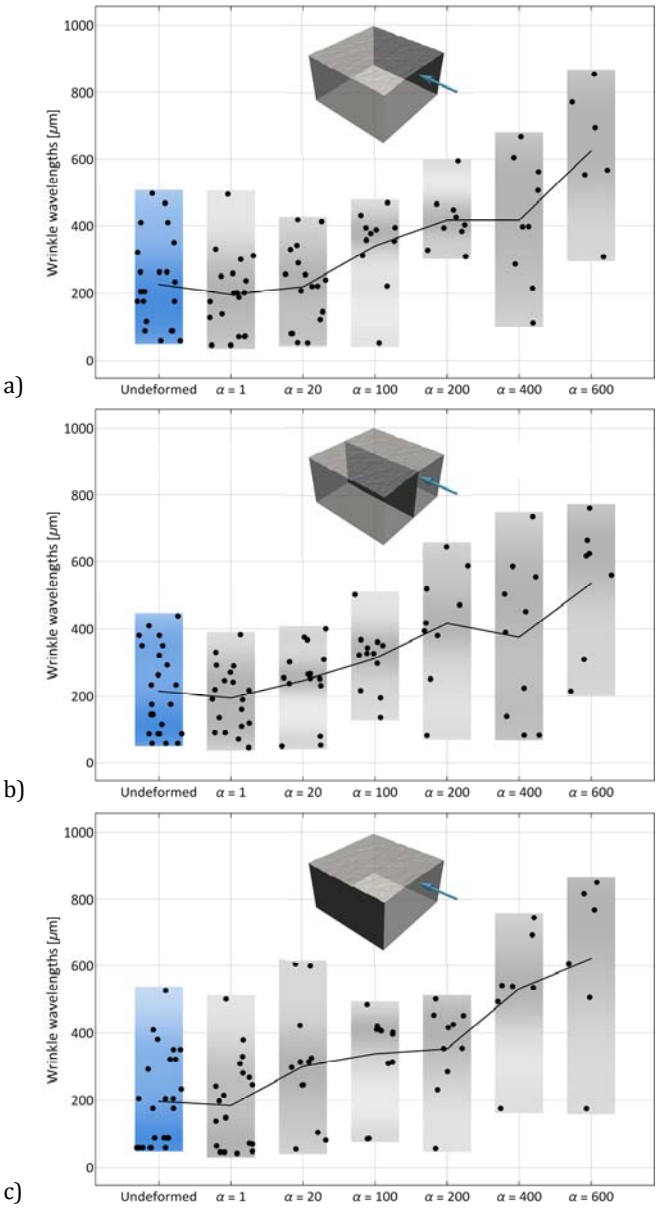

Figure 9 Statistical distribution of wrinkle wavelengths along 3 profiles of the *stratum corneum surface* [(a) y = -2.5 mm; b) y = 0 mm; c) y = 2.5 mm] as a function of the stiffness ratio α after 25% compression. The distribution of wavelengths in the undeformed configuration are also plotted (dark pink). Black lines join the median values of each distribution.

Based on the modelling framework of their multi-stage buckling theory, Kuwazuru et al.[69] suggested that wrinkle morphology suddenly changes from *stratum corneum* wrinkling to epidermis wrinkling leading respectively to shallow fine furrows (i.e. micro-wrinkles according to our naming convention) and deep coarse wrinkles. These authors later designed an experimental apparatus to test this hypothesis[34]. They showed that the skin wrinkling rate experiences a step increase at the age of 33 translating into a sudden change in the morphology of skin wrinkles.

What these authors called "buckling mode switch" is the result of what had already been explained by Cerda and Mahadevan[22], namely the competition between bending energies of individual layers which favour particular wave lengths during wrinkle formation.

The ratio of bending energies is conditioned by the geometry and material properties of individual layers. Any alteration of these properties, for example as a result of the ageing process or alterations in relative humidity conditions, will affect the morphology of wrinkles. This is clearly illustrated in our study. More recently, Shiihara et al.[70] designed a series of finite element analyses to study the effect of skin microrelief on large wrinkles. Their simplified two-dimensional analyses were based on a highly idealised skin microrelief and dynamic implicit-based buckling-post-buckling procedures[58]. It was suggested that fine microrelief at the surface inhibit large wrinkles (i.e. deeper than 0.35 mm). In our three-dimensional anatomically-based series of analyses we found that inhibition of deep wrinkles only occurs for moderate layer stiffness ratios.

Theoretical analysis of a neo-Hookean bi-layer structure

Cao and Hutchinson[24] extended Biot's exact finite strain bifurcation analysis to a compressed planar bi-layer structure made of a thin film ($\bullet_f$) laying on top of an infinitely thick substrate ($\bullet_s$);They showed that, for both layers in a stress-free reference state, the compressive bifurcation strain at the onset of wrinkling matches very well that determined by Allen[71] who considered the film to be linear elastic provided the modulus ratio $\alpha = \mu_f / \mu_s$ is large enough (>10). In these conditions, the compressive bifurcation strain ε_0 can be estimated as:

$$\varepsilon_0 = \frac{1}{4}\left(\frac{3\mu_s}{\mu_f}\right)^{\frac{2}{3}} \quad (4)$$

while the critical wave number is:

$$k_0 = \frac{1}{h}\sqrt[3]{\frac{3\mu_s}{\mu_f}} \quad (5)$$

leading to a wrinkle wave length λ_0:

$$\lambda_0 = \frac{2\pi}{k_0} = 2\pi h \sqrt[3]{\frac{\mu_f}{3\mu_s}} \quad (6)$$

By inserting the value of the *stratum corneum* thickness that was used in the finite element analyses ($h = 20$ μm) into equation (6), the theoretical critical wavelength predicted by Cao and Hutchinson[24] was plotted (**Figure 10**).

By comparing **Figure 9** and **Figure 10** it is clear that the numerical solutions of the anatomical skin model are in very good agreement with theoretical solutions for an idealised (i.e. planar) equivalent structure. However, it is relevant to point out that the numerical solutions correspond to post-bifurcation states following application of a 25% macroscopic compressive strain while theoretical values pertain to the critical bifurcation threshold.

To assess whether significant strains are induced in the *stratum corneum*[47], and therefore to shed light on the balance between structural and material deformation mechanisms, the apparent stretch along the compression direction of 172 vertical profiles of the skin surface (each corresponding to a row of nodes from the structured finite element grid) was calculated for each value of α (**Figure 11**).

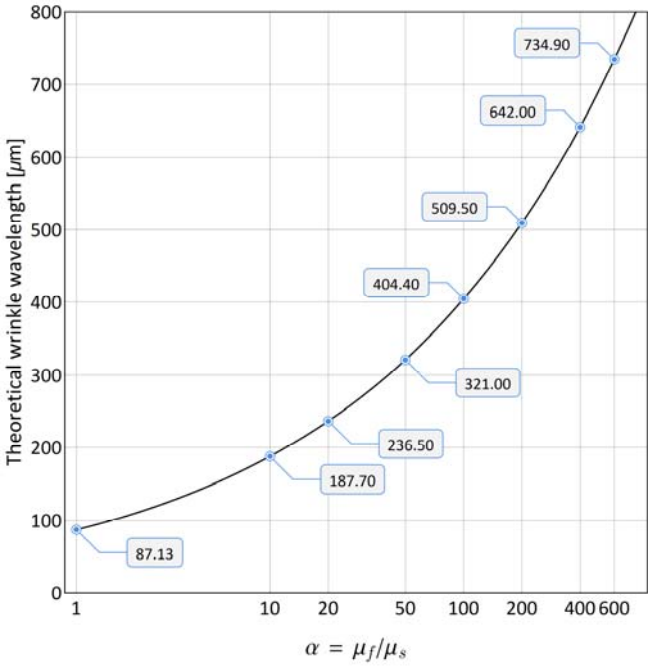

Figure 10 Theoretical critical wrinkle wavelength for a neo-Hookean bi-layer structure made of a 20 μm thick thin film lying on an infinitely deep substrate as a function of the ratio of their respective shear moduli α [Equation (6)].

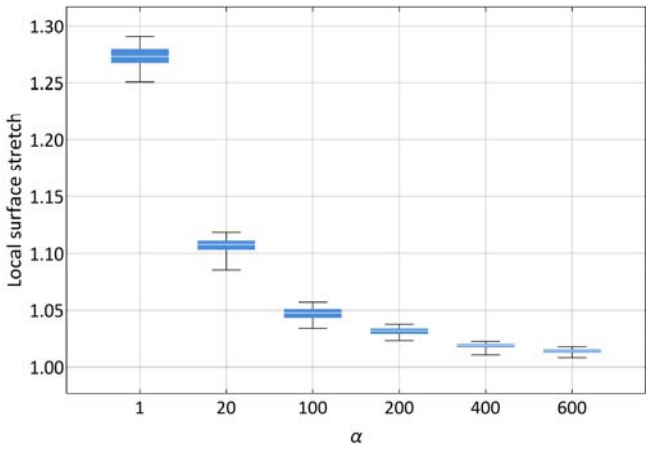

Figure 11 Statistical distribution of stretches at the external surface of the stratum corneum after application of a uniform 25% macroscopic compressive strain as a function of the stiffness ratio α (n = 172).

When the *stratum corneum* and substrate feature the same material properties, surface strains in excess of 25% are induced in the *stratum corneum* while these values drop to around 10% when the stiffness ratio α increases by a factor of 20 (Figure 11).

For α ranging from 100 to 600, surface strains are roughly under 5%. This shows that for moderate stiffness ratios, it is essential to use finite strain theory.

4 Conclusion

Understanding the biophysics of skin wrinkling is of critical importance in cosmetics, dermatology, and surgery. Throughout the past decade, bi-layered model systems have evolved as a valuable tool to study the mechanisms of skin wrinkling in idealised two-dimensional geometries. However, these idealised systems can only generate regular wrinkling patterns and fail to accurately predict the surface topology of real human skin. Here we reconstructed the microrelief of a 0.25 cm^2 skin patch using laser scanning profilometry to characterise the impact of initial surface imperfections on pattern formation upon compression-induced wrinkling. We modelled the skin patch as a bi-layered system with a 20 μm thick *stratum corneum* layer on top of a 2.6mm thick skin substrate. In a systematic sensitivity analysis, we studied the effects of a fully three-dimensional microrelief geometry on wrinkling pattern formation for different stiffness ratios between layer and substrate. Strikingly, for moderate stiffness ratios up to 20, and for the particular surface considered, external compression simplify magnifies the underlying microrelief pattern. It is worth to reiterate that such a result was obtained for a single skin microrelief sample. There is a strong intra- and inter-individual variability in the material and structural properties of the skin, particularly across the life course. Ageing can significantly alter the skin microstructure, whether at its surface or deeper within the epidermal and dermal layers. Future studies should look at quantifying the effects of microrelief geometry (e.g. glyphic pattern orientation and density) and internal microstructure on wrinkle formation, particularly for moderate layer stiffness ratios. For stiffness ratios larger than 100, external compression induces a well-defined periodic wrinkling pattern at wavelengths that agree well with analytical predictions. While analytical models and computational simulations of idealised model systems provide valuable insight into the wrinkling pattern of regular structures at high stiffness contrasts, they cannot predict surface topologies of realistic skin surfaces with irregular microstructures. Especially for human skin with an inherently irregular surface topology, realistic three-dimensional modelling can become critically important since surface instabilities are highly sensitive to initial imperfections. Our next steps towards more physiological modelling are to also include the effects of tissue anisotropy and residual stress. Our sensitivity analysis with varying *stratum corneum* stiffnesses has important implications in understanding the effects of drying or ageing on altered surface pattern formation.

Acknowledgements

Georges Limbert would like to gratefully acknowledge the University of Southampton for the award of an Internationalisation Fund grant. This funding enabled a visit to Stanford University during which discussions that led to this paper were initiated.

References

1. G. E. Piérard, I. Uhoda and C. Piérard-Franchimont, *J Cosm Derm*, 2004, **2**, 21-28.
2. R. Bridson, S. Marino and R. Fedkiw, Proceedings of the 2003 ACM SIGGRAPH/Eurographics symposium on Computer Animation, San Diego, CA, USA, 2003, 28-36.
3. N. Magnenat-Thalmann, P. Kalra, J. L. Lévêque, R. Bazin, D. Batisse and B. Querleux, *IEEE Trans Inf Technol Biomed*, 2002, **6**, 317-323.
4. D. Rohmer, T. Popa, M.-P. Cani, S. Hahmann and A. Sheffer, *ACM Trans. Graph.*, 2010, **29**, 1-8.
5. Y. Wu, P. Kalra, L. Moccozet and N. Magnenat-Thalmann, *Visual Comp.*, 1999, **15**, 183-198.
6. G. Limbert, *P Roy Soc A-Math Phys*, 2017, **473**, 1-39.
7. A. Gefen, *J Tissue Viability*, 2011, **20**, 81-88.
8. S. Derler and L. C. Gerhardt, *Trib Lett*, 2012, **45**, 1-27.
9. I. Hoogendoorn, J. Reenalda, B. F. J. M. Koopman and J. S. Rietman, *J Tissue Viability*, 2017, **26**, 157-171.
10. M. F. Leyva-Mendivil, J. Lengiewicz, A. Page, N. W. Bressloff and G. Limbert, *Trib Lett*, 2017, **65**, 12.
11. M. F. Leyva-Mendivil, J. Lengiewicz, A. Page, N. W. Bressloff and G. Limbert, *Biotribology*, 2017, **11**, 110-123.
12. M. J. Adams, B. J. Briscoe and S. A. Johnson, *Trib Lett*, 2007, **26**, 239-253.
13. M. F. Leyva-Mendivil, J. Lengiewicz and G. Limbert, *Surface Topography: Metrology and Properties*, 2017, available online.
14. N. K. Veijgen, M. A. Masen and E. van der Heide, *J Mech Behav Biomed Mater*, 2013, **28**, 448-461.
15. M. Ramos-e-Silva and S. C. da Silva Carneiro, *J Cosm Derm*, 2007, **6**, 40-50.
16. H. Assaf, M. A. Adly and M. R. Hussein, in *Textbook of Aging Skin*, eds. M. A. Farage, K. W. Miller and H. I. Maibach, 2010, ch. 13, pp. 129-138.
17. K. S. Wu, W. W. van Osdol and R. H. Dauskardt, *Biomaterials*, 2006, **27**, 785-795.
18. S. Wang, M. Li, J. Wu, D.-H. Kim, N. Lu, Y. Su, Z. Kang, Y. Huang and J. A. Rogers, *J Appl Mech*, 2012, **79**, 031022-031022.
19. E. Lejeune, A. Javili and C. Linder, *Extreme Mechanics Letters*, 2016, **7**, 10-17.
20. H. Shimizu, *Shimizu's Textbook of Dermatology*, Hokkaido University Press - Nakayama Shoten Publishers, 2007.
21. Y. Lanir, in *Handbook of Bioengineering*, eds. R. Skalak and S. Chien, McGraw-Hill, New York, 1987.
22. E. Cerda and L. Mahadevan, *Phys. Rev. Lett.*, 2003, **90**, 074302-074301:074302-074304.
23. S. Budday, E. Kuhl and J. W. Hutchinson, *Philosophical magazine (Abingdon, England)*, 2015, **95**, 3208-3224.
24. Y. Cao and J. W. Hutchinson, *J Appl Mech*, 2012, **79**, 0310191-0310199.
25. K. Efimenko, M. Rackaitis, E. Manias, A. Vaziri, L. Mahadevan and J. Genzer, *Nat Mater*, 2005, **4**, 293-297.
26. J. Genzer and J. Groenewold, *Soft Matter*, 2006, **2**, 310-323.

27. A. Goriely, M. Destrade and M. Ben Amar, *Q J Mech Appl Math*, 2006, **59**, 615-630.
28. M. A. Holland, B. Li, X. Q. Feng and E. Kuhl, *J Mech Phys Solids*, 2017, **98**, 350-365.
29. Y. Cao and J. W. Hutchinson, *P Roy Soc A-Math Phys*, 2012, **468**, 94-115.
30. R. Zhao and X. Zhao, *J Appl Mech*, 2017, **84**, 081001-081001-081013.
31. P. Ciarletta, M. Destrade and A. L. Gower, *The Quarterly Journal of Mechanics and Applied Mathematics*, 2013, **66**, 273-288.
32. J.-Y. Sun, S. Xia, M.-W. Moon, K. H. Oh and K.-S. Kim, *P Roy Soc A-Math Phys*, 2012, **468**, 932-953.
33. T. Tallinen, J. Y. Chung, J. S. Biggins and L. Mahadevan, *PNAS*, 2014, **111**, 12667-12672.
34. O. Kuwazuru, K. Miyamoto, N. Yoshikawa and S. Imayama, *Skin Res Technol*, 2012, **18**, 495-503.
35. C. O. Flynn and B. A. O. McCormack, *Comput Meth Biomech Biomed Eng*, 2009, **12**, 125-134.
36. C. O. Flynn and B. A. O. McCormack, *J Biomech*, 2010, **43**, 442-448.
37. A. M. Kligman, P. Zheng and R. M. Lavker, *Br J Derm*, 1985, **113**, 37-42.
38. D. Pond, A. McBride, L. Davids, B. D. Reddy and G. Limbert, *J Theor Biol*, 2017, **under review**.
39. G. E. Piérard, J. F. Hermanns and C. H. Lapière, *Dermatologica*, 1974, **149**, 266-273.
40. C. Piérard-Franchimont and G. E. Piérard, *Am J Dermopathol*, 1987, **9**, 500-509.
41. M. Setaro and A. Sparavigna, *Skin Res Technol*, 2001, **7**, 159-163.
42. J. L. Lévêque, *J Eur Acad Derm Vener*, 1999, **12**, 103-114.
43. J. L. Lévêque and B. Audoly, *Skin Res Technol*, 2013, **19**, 42-46.
44. K. Hashimoto, *International Journal of Dermatology*, 1974, **13**, 357-381.
45. P. Quatresooz, L. Thirion, C. Piérard-Franchimont and G. E. Piérard, *International Journal of Cosmetic Science*, 2006, **28**, 389-395.
46. H. Zahouani, G. Boyer, C. Pailler-Mattei, M. Ben Tkaya and R. Vargiolu, *Wear*, 2011, **271**, 2364-2369.
47. M. F. Leyva-Mendivil, A. Page, N. W. Bressloff and G. Limbert, *J Mech Behav Biomed Mater*, 2015, **49**, 197-219.
48. K. Levi and R. H. Dauskardt, *International Journal of Cosmetic Science*, 2010, **32**, 294-298.
49. K. Levi, R. J. Weber, J. Q. Do and R. H. Dauskardt, *International Journal of Cosmetic Science*, 2010, **32**, 276-293.
50. R. Marks and A. D. Pearse, *Br J Derm*, 1975, **92**, 651-657.
51. J. Hatzis, *Micron*, 2004, **35**, 201-219.
52. G. K. Menon, G. W. Cleary and M. E. Lane, *International Journal of Pharmaceutics*, 2012, **435**, 3-9.
53. A. M. Zöllner, A. Buganza Tepole and E. Kuhl, *J Theor Biol*, 2012, **297**, 166-175.
54. J. E. Marsden and T. J. R. Hughes, *Mathematical Foundations of Elasticity*, Dover, New-York, 1994.
55. E. A. de Souza Neto, D. Perić, M. Dutko and D. R. J. Owen, *Int J Solids Struct*, 1996, **33**, 3277-3296.
56. J. Korelc, *Eng. Comput.*, 2002, **18**, 312-327.
57. J. Korelc and P. Wriggers, *Automation of Finite Element Methods*, Springer, , First edn., 2016.
58. Y. W. Wong and S. Pellegrino, *Journal of Mechanics of Materials and Structures*, 2006, **1**, 61-93.
59. E. A. de Souza Neto and Y. T. Feng, *Comput Meth Appl Mech Eng*, 1999, **179**, 81-89.
60. B. Cochelin, *Comput. Struct.*, 1994, **53**, 1181-1192.
61. B. Dortdivanlioglu, A. Javili and C. Linder, *Comput Meth Appl Mech Eng*, 2016, **316**, 261-279.
62. L. Chen, N. Nguyen-Thanh, H. Nguyen-Xuan, T. Rabczuk, S. P. A. Bordas and G. Limbert, *Comput Meth Appl Mech Eng*, 2014, **277**, 104-130.
63. A. Buganza Tepole, H. Kabaria, K.-U. Bletzinger and E. Kuhl, *Comput Meth Appl Mech Eng*, 2015, **293**, 328-347.
64. A. Javili, P. Steinmann and E. Kuhl, *J Mech Behav Biomed Mater*, 2014, **29**, 20-32.
65. N. M. Newmark, *Journal of the Engineering Mechanics Division*, 1959, **85**, 67-94.
66. Y. Zhao, Y. Cao, W. Hong, M. K. Wadee and X.-Q. Feng, *Towards a quantitative understanding of period-doubling wrinkling patterns occurring in film/substrate bilayer systems*, 2015.
67. E. S. Gadelmawla, M. M. Koura, T. M. A. Maksoud, I. M. Elewa and H. H. Soliman, *J. Mater. Process. Technol.*, 2002, **123**, 133-145.
68. Mathematica® v11.2 FindPeaks function, http://reference.wolfram.com/language/ref/FindPeaks.html, (accessed 19/12/2017, 2017).
69. O. Kuwazuru, J. Saothong and N. Yoshikawa, *Med Eng Phys*, 2008, **30**, 516-522.
70. Y. Shiihara, M. Sato, Y. Hara, I. Iwai and N. Yoshikawa, *Skin Res Technol*, 2014, **0**, 1-8.
71. H. G. Allen, in *Analysis and Design of Sandwich Panels*, Pergamon, New York, 1969, pp. 156-189.